PIER C

A Spatial Electromagnetic Field Analysis Method for Estimating the Dynamic Positions of Multiple Mobile High-Frequency Power Supplies

Rui Zhang*, Yanfeng Gao, and Jixuan Wang

Institute of Water Conservancy and Hydroelectric Power, Hebei University of Engineering, Handan, China

ABSTRACT: A spatial electromagnetic field analysis method is proposed by adding variable speed nodes to the circuit topology to estimate the optimal location of multiple mobile high-frequency power supplies at multiple nodes in this paper. In the process of continuous motion, the speed and position of motion affect the accumulated power and loss at the circuit node. At the same time, the transmission efficiency and delay characteristics of the high-frequency mobile power supply will also change with the precise positioning of the mobile power supply and the change of the spatially coupled electromagnetic field. The spatial electromagnetic field analysis method with variable speed nodes is used to divide the circuit topology of mobile high frequency power supply system according to the number of nodes. The continuous motion of variable speed nodes is used to simulate the real-time positioning of multiple mobile high-frequency power sources. By analyzing the real-time variation of the high-frequency electromagnetic field at variable speed nodes, the quantitative relationship between the electromagnetic characteristics of the node space and the speed and positioning of the mobile power supply is established. Finally, the fast optimal positioning of each mobile high-frequency power supply in the continuous moving process is obtained. Compared with the position estimation results obtained by the traditional relation calculation method, when the size is greater than 100, the proposed method can locate the position of multi-mobile high-frequency power supply faster and more accurately, and the circuit efficiency reaches 90%. The simulation results verify the correctness of the theoretical analysis.

1. INTRODUCTION

With the wide application of mobile high-frequency power supply in energy, power, wireless communication, and other fields, flexible power supply system is in high demand. For improving the flexibility of power supply system, multi-mobile high-frequency power supply system can provide emergency response and ensure the safe operation of the system. However, in the process of continuous movement of the high-frequency power supply, the moving speed and position affect the accumulated power and loss at the circuit node. At the same time, the transmission efficiency and delay characteristics of the high-frequency mobile power will also change with the change of the precise positioning of the mobile power and the spatially coupled electromagnetic field. Therefore, it is necessary to propose a fast analysis method to obtain the normal optimal positioning of multi-mobile high-frequency power supply system in real time, so as to improve the power supply efficiency and reliability of the system, reduce the path loss of mobile power, and shorten the transmission delay characteristics of power. A novel spatial electromagnetic field analysis method is presented. This method considers the continuous variable speed movement of the circuit nodes, divides the circuit topology of mobile high-frequency power supply system according to the number of nodes, and simulates the real-time location of multiple mobile high-frequency power supplies

through the continuous movement of nodes. By analyzing the real-time variation of the high-frequency electromagnetic field at variable speed nodes, the quantitative relationship between the electromagnetic characteristics of node space and the speed and position of the mobile power supply is established. Finally, the fast optimal location of each mobile high-frequency power supply in the system under normal conditions is obtained.

At present, there are many researches on mobile power system under special environmental conditions. They mainly focus on the stability of mobile power supply system [1–4], capacity reliability, and elastic power supply [5–7]. However, the method adopted in special working conditions is not suitable for normal working conditions under long-term operation of the system. Considering the influence of multi-source and circuit topology energy consumption constraints, research contents such as cost efficiency calculation and nonlinear energy collection theory of the mobile power system can meet the constraints of the system [8–10]. Considering the addition of mobile storage system, multi-objective collaborative optimization and mobile energy production and storage optimization are also analyzed from the perspective of the system [11, 12], but the self-positioning optimization of multi-source and multi-node mobile power supply has not been fundamentally studied. Especially for high-frequency mobile power supplies, frequent positioning data requires more accurate optimization algorithms [13]. Considering dynamic factors, dynamic charging optimization of mobile charging stations in the Internet of

* Corresponding author: Rui Zhang (ztlyaodi17@163.com).

Things environment, dynamic charging pricing methods, joint routing and charging framework of energy balance in the network [14–16] all take dynamic factors into account in the direction of mobile charging energy optimization. However, the influence of dynamic electromagnetic characteristics of mobile power on charging optimization has not been studied. Dynamic electromagnetic characteristic parameters also increase path loss in circuit topology and have transmission delay characteristics [17]. The location space electromagnetic characteristics are considered, including the spatial framework for strategic placement of the power system, electromagnetic wave selection for multi-size device power supply, and electromagnetic noise analysis of switching power modules [18–21], but the research content lacks the spatial electromagnetic wave characteristics analysis of mobile power modules. Especially for the multi-node high-frequency mobile power supply system, the electromagnetic parameters of space nodes brought about by spatial electromagnetic wave coupling also affect the positioning optimization of mobile power supply [22–24].

Therefore, there are relatively few researches on dynamic spatial electromagnetic characteristics of physical field coupling in mobile high frequency power supply systems with multiple continuous moving circuit nodes. At the same time, there are relatively few researches on the combination of dynamic parameters of circuit topology with node output power and dynamic power flow output characteristics. In order to analyze the influence of the position change and displacement rate of multiple mobile high-frequency power supplies on the output power and efficiency of each node in the system, a spatial electromagnetic field analysis method with variable speed circuit nodes is proposed to obtain the real-time optimal positioning of multiple mobile high-frequency power supplies under normal conditions.

2. THE SPATIAL ELECTROMAGNETIC FIELD DISTRIBUTION

In order to solve the influence of the spatial node electromagnetic parameter change on the precise location of the mobile power supply due to the variable speed movement of the power supply, a spatial electromagnetic field analysis method of variable speed node is proposed to study this problem. Firstly, Maxwell's equations can be used to describe the electromagnetic coupling of complex circuits. Among them, the electromagnetic coupling relationship is related to the spatial frequency and field parameters of the location of circuit. On the contrary, the optimization of circuit parameters, transmission power, and dynamic power can be solved according to the influence of location spatial frequency and field parameters on conductors and circuits [25].

Set the presence state of a simple circuit in space to a rectangle with length a and width b. Take the center of the rectangular space as the origin of coordinates, as shown in Fig. 1. Voltage V is applied to the circuit, and current I flows through the loop. The spatial electromagnetic field around the loop generates an induced current I' in the direction opposite to the current I at each of the four boundaries of the rectangular circuit.
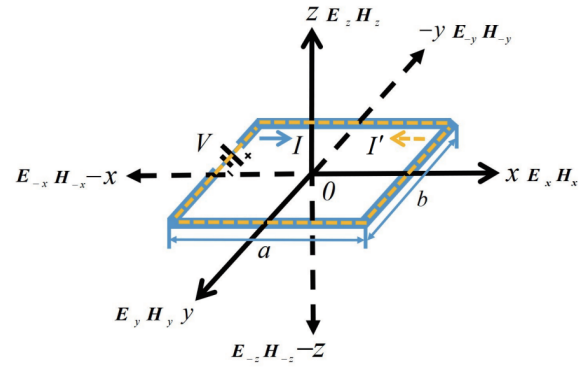
FIGURE 1. Space electromagnetic field coordinate system of rectangular circuit.

Available from Equation (1),

$$
\begin{cases}
\nabla \times \mathbf{H}\left(\mathbf{r}, t\right) = \sigma \mathbf{E}\left(\mathbf{r}, t\right) + \dfrac{\partial \varepsilon \mathbf{E}\left(\mathbf{r}, t\right)}{\partial t} \\[2mm]
\nabla \times \mathbf{E}\left(\mathbf{r}, t\right) = -\dfrac{\partial \mu \mathbf{H}\left(\mathbf{r}, t\right)}{\partial t} \\[2mm]
\nabla \times \nabla \times \mathbf{E}\left(\mathbf{r}, t\right) = -\sigma \mu \dfrac{\partial \mathbf{E}\left(\mathbf{r}, t\right)}{\partial t} - \varepsilon \mu \dfrac{\partial^2 \mathbf{E}\left(\mathbf{r}, t\right)}{\partial t^2} \\[2mm]
\nabla \times \nabla \times \mathbf{H}\left(\mathbf{r}, t\right) = -\sigma \mu \dfrac{\partial \mathbf{H}\left(\mathbf{r}, t\right)}{\partial t} - \varepsilon \mu \dfrac{\partial^2 \mathbf{H}\left(\mathbf{r}, t\right)}{\partial t^2}
\end{cases}
\tag{1}
$$

The components of electric and magnetic field vector on coordinate axis are: $\mathbf{E_x}$, $\mathbf{E_y}$, $\mathbf{E_z}$, $\mathbf{E_{-x}}$, $\mathbf{E_{-y}}$, $\mathbf{E_{-z}}$ and $\mathbf{H_x}$, $\mathbf{H_y}$, $\mathbf{H_z}$, $\mathbf{H_{-x}}$, $\mathbf{H_{-y}}$, $\mathbf{H_{-z}}$. In Fig. 1, the center coordinate of the rectangular space is 0. The induced magnetic field is divided into two parts in Fig. 2(a). One is the magnetic field distribution around the four boundaries of the rectangular loop, such as $\mathbf{H}_{-a/2 \leq x \leq a/2,\, y=\pm b/2}$, $\mathbf{H}'_{-a/2 \leq x \leq a/2,\, y=\pm b/2}$, $\mathbf{H}_{-b/2 \leq y \leq b/2,\, x=\pm a/2}$, $\mathbf{H}'_{-b/2 \leq y \leq b/2,\, x=\pm a/2}$, and the other is the magnetic field distribution through the center of the loop along the radial symmetry, such as $\mathbf{H}_{-a/2 \leq x \leq a/2,\, -b/2 \leq y \leq b/2,\, z>0}$, $\mathbf{H}'_{-a/2 \leq x \leq a/2,\, -b/2 \leq y \leq b/2,\, z>0}$, $\mathbf{H}_{-a/2 \leq x \leq a/2,\, -b/2 \leq y \leq b/2,\, z<0}$, $\mathbf{H}'_{-a/2 \leq x \leq a/2,\, -b/2 \leq y \leq b/2,\, z<0}$. The induced electric field is also divided into two parts in Fig. 2(b). One is the electric field distribution along the boundary at the four boundaries of the rectangular loop, such as $\mathbf{E}_{-a/2 \leq x \leq a/2,\, y=\pm b/2}$, $\mathbf{E}'_{-a/2 \leq x \leq a/2,\, y=\pm b/2}$, $\mathbf{E}_{-b/2 \leq y \leq b/2,\, x=\pm a/2}$, $\mathbf{E}'_{-b/2 \leq y \leq b/2,\, x=\pm a/2}$, and the other is the electric field distribution along the symmetric axis at the center of the loop, such as $\mathbf{E}_{-a/2 \leq x \leq a/2,\, -b/2 \leq y \leq b/2,\, z=0}$, $\mathbf{E}'_{-a/2 \leq x \leq a/2,\, -b/2 \leq y \leq b/2,\, z=0}$.

Arrows and symbols are used to represent the distribution of spatial electromagnetic field at the boundary of the rectangular circuit and in the loop. It can be seen from Fig. 2 that the spatial electric field and spatial magnetic field are expressed in the figure as two parts at the boundary and in the loop, respectively, and the resulting spatial electromagnetic field has a coupling relationship. The spatial electromagnetic field distribution of the
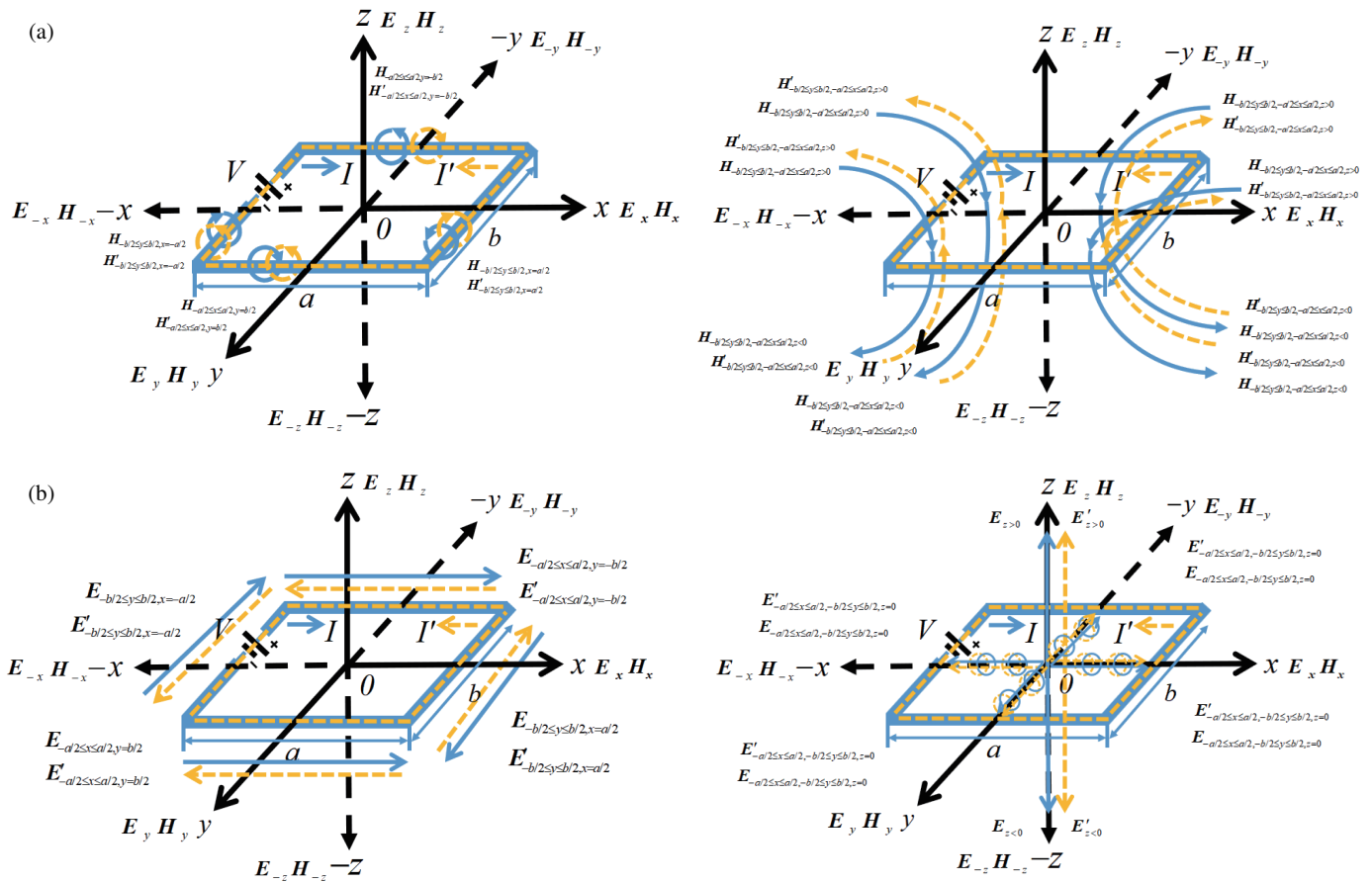
FIGURE 2. (a) Spatial magnetic field distribution at the boundary of a rectangular circuit and within the loop. (b) Spatial electric field distribution at the boundary of the rectangular circuit and in the loop.

two parts can be solved and located in the spatial coordinate system. At the same time, the induced electromagnetic field at the boundary will change the parameters of the original circuit, which will cause the value of the current in the original circuit to change.

The analysis of the effect of spatial electromagnetic field distribution on circuit parameters and current flow value can be converted into the analysis of real-time position change. The analysis principle of the two equivalent influence characteristics is shown in Fig. 3.

In Fig. 3, a simple circuit is taken as an example. The whole circuit is divided by four nodes, numbered 1, 2, 3, 4, to simulate the influence of spatial electromagnetic field distribution, and the equivalent mobile power is added to analyze the influence of seven different positions on the circuit current flow.

In the (1) position, the equivalent mobile power supply V_{12} is added between nodes 1 and 2, and the induced current I', circuit current I_L, and efficiency η (ratio of output power to input power) in the circuit circuit are respectively:

$$\begin{cases} I' = I_{21} \\ I_L = I - I' = I - I_{21} \\ \eta = \frac{I_L}{I} = \frac{I - I_{21}}{I} = 1 - \frac{I_{21}}{I} \end{cases} \quad (2)$$

In the (2) position, the equivalent mobile power supply V_{23} is added between nodes 2 and 3, and the induced current I', circuit current I_L, and efficiency η (ratio of output power to input power) in the circuit circuit are respectively:

$$\begin{cases} I' = I_{32} \\ I_L = I - I' = I - I_{32} \\ \eta = \frac{I_L}{I} = \frac{I - I_{32}}{I} = 1 - \frac{I_{32}}{I} \end{cases} \quad (3)$$

In the (3) position, the equivalent mobile power supply V_{34} is added between nodes 3 and 4, and the induced current I', circuit current I_L, and efficiency η (ratio of output power to input power) in the circuit circuit are respectively:

$$\begin{cases} I' = I_{43} \\ I_L = I - I' = I - I_{43} \\ \eta = \frac{I_L}{I} = \frac{I - I_{43}}{I} = 1 - \frac{I_{43}}{I} \end{cases} \quad (4)$$

In the (4) position, the equivalent mobile power supplies V_{23} and V_{34} are added between nodes 2, 3 and 3, 4, and the induced current I', circuit current I_L, and efficiency η (ratio of output power to input power) in the circuit circuit are respectively:

$$\begin{cases} I' = I_{43} + I_{32} \\ I_L = I - I' = I - I_{43} - I_{32} \\ \eta = \frac{I_L}{I} = \frac{I - I_{43} - I_{32}}{I} = 1 - \frac{I_{43}}{I} - \frac{I_{32}}{I} \end{cases} \quad (5)$$
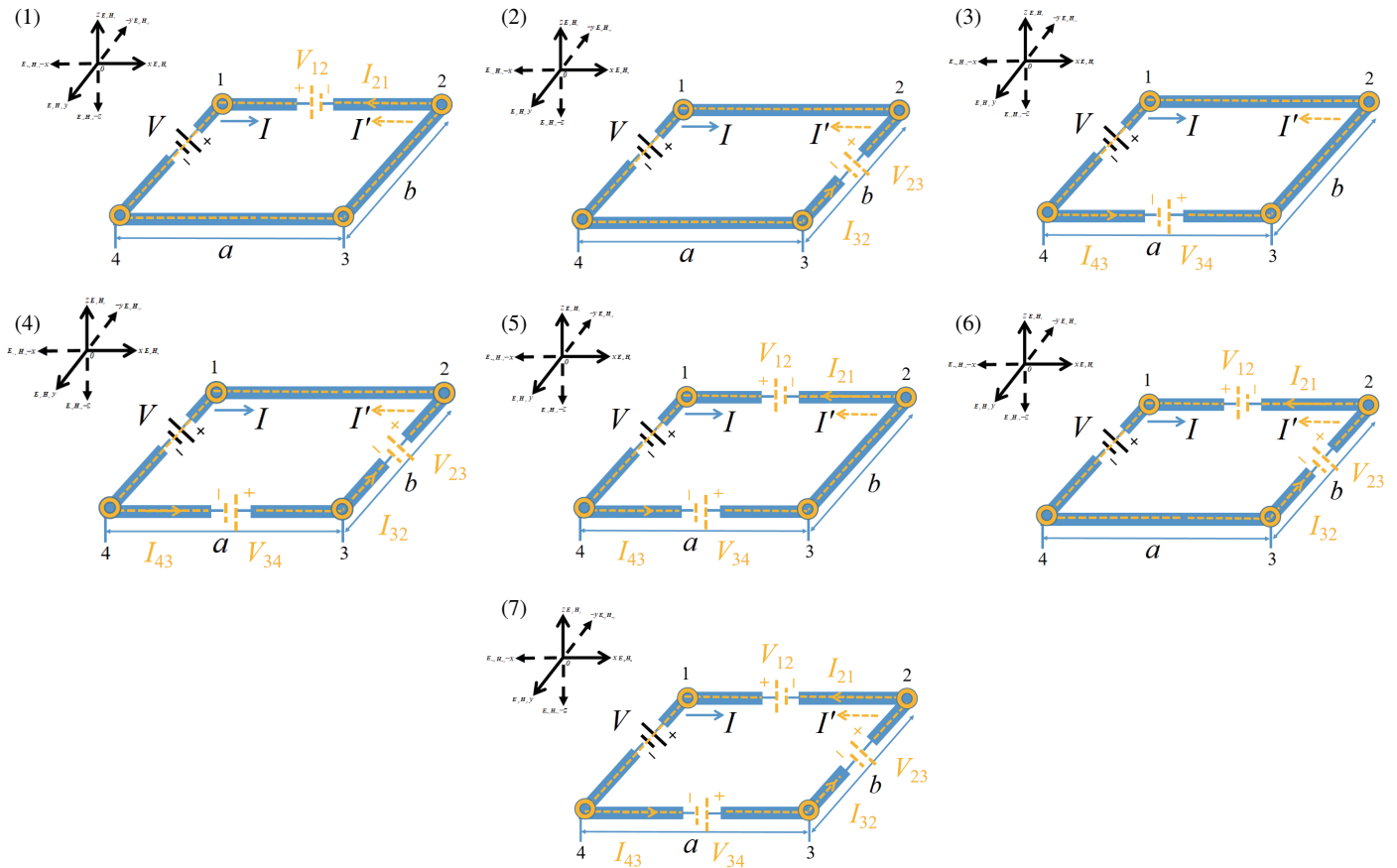
FIGURE 3. Influence of 7 different position distributions of equivalent power supply and circuit current variation.

In the (5) position, the equivalent mobile power supplies V_{12} and V_{34} are added between nodes 1, 2 and 3, 4, and the induced current I', circuit current I_L, and efficiency η (ratio of output power to input power) in the circuit circuit are respectively:

$$\begin{cases} I' = I_{43} + I_{21} \\ I_L = I - I' = I - I_{43} - I_{21} \\ \eta = \frac{I_L}{I} = \frac{I - I_{43} - I_{21}}{I} = 1 - \frac{I_{43}}{I} - \frac{I_{21}}{I} \end{cases} \quad (6)$$

In the (6) position, the equivalent mobile power supplies V_{12} and V_{23} are added between nodes 1, 2 and 2, 3, and the induced current I', circuit current I_L, and efficiency η (ratio of output power to input power) in the circuit circuit are respectively:

$$\begin{cases} I' = I_{21} + I_{32} \\ I_L = I - I' = I - I_{21} - I_{32} \\ \eta = \frac{I_L}{I} = \frac{I - I_{21} - I_{32}}{I} = 1 - \frac{I_{21}}{I} - \frac{I_{32}}{I} \end{cases} \quad (7)$$

In the (7) position, the equivalent mobile power supplies V_{12}, V_{23}, and V_{34} are added between nodes 1, 2, 2, 3 and 3, 4, and the induced current I', circuit current I_L, and efficiency η (ratio of output power to input power) in the circuit circuit are respectively:

$$\begin{cases} I' = I_{21} + I_{32} + I_{43} \\ I_L = I - I' = I - I_{21} - I_{32} - I_{43} \\ \eta = \frac{I_L}{I} = \frac{I - I_{21} - I_{32} - I_{43}}{I} = 1 - \frac{I_{21}}{I} - \frac{I_{32}}{I} - \frac{I_{43}}{I} \end{cases} \quad (8)$$

From the analysis of the induced current, current flow, and efficiency of the above seven different positions, it is concluded that with the difference and increase of the equivalent mobile power supply position, the induced current increases; the current flow decreases; and the efficiency also decreases. In addition, the spatial electromagnetic field distribution around the circuit can provide the analysis basis for the real-time location of the power supply.

First of all, take Fig. 3 as an example, in the conversion sequence of 7 different positions, assuming that the impedance per meter in the rectangular circuit is Z_L, and the estimated position x, y, and z of the equivalent mobile power supply can be obtained respectively:

For position (1), the equivalent mobile power supply V_{12} is added between nodes 1 and 2, then the estimated position x of V_{12} from node 1 is:

$$\begin{cases} \dfrac{V_{12}}{xZ_L} = \dfrac{V - V_{12}}{(2a + b - x)\,Z_L} \\ x = \dfrac{(2a + b)\,V_{12}}{V} \end{cases} \quad (9)$$

For position (2), the equivalent mobile power supply V_{23} is added between nodes 2 and 3, then the estimated position x of

V_{23} from node 2 is:

$$\begin{cases} \dfrac{V_{23}}{xZ_L} = \dfrac{V - V_{23}}{(2a + b - x)\,Z_L} \\[3mm] x = \dfrac{(2a + b)\,V_{23}}{V} \end{cases} \tag{10}$$

For position (3), the equivalent mobile power supply V_{34} is added between nodes 3 and 4, then the estimated position x of V_{34} from node 3 is:

$$\begin{cases} \dfrac{V_{34}}{xZ_L} = \dfrac{V - V_{34}}{(2a + b - x)\,Z_L} \\[3mm] x = \dfrac{(2a + b)\,V_{34}}{V} \end{cases} \tag{11}$$

For position (4), the equivalent mobile power supplies V_{23} and V_{34} are added between nodes 2, 3 and 3, 4. Then, the estimated position of V_{23} from node 2 is x, and the estimated position of V_{34} from node 3 is y. Assuming $y = kx$, the values of x and y are as follows:

$$\begin{cases} \dfrac{V_{23}}{xZ_L} + \dfrac{V_{34}}{yZ_L} = \dfrac{V - V_{23} - V_{34}}{(a + b - x + a - y)\,Z_L} \\[3mm] y = kx \end{cases} \Rightarrow$$

$$\begin{cases} x = \dfrac{(2a + b)\,(kV_{23} + V_{34})}{k^2 V_{23} + kV + V_{34}} \\[3mm] y = \dfrac{(2a + b)\,(k^2 V_{23} + kV_{34})}{k^2 V_{23} + kV + V_{34}} \end{cases} \tag{12}$$

For position (5), the equivalent mobile power supplies V_{12} and V_{34} are added between nodes 1, 2 and 3, 4. Then, the estimated position of V_{12} from node 1 is x, and the estimated position of V_{34} from node 3 is y. Assuming $y = kx$, the values of x and y are as follows:

$$\begin{cases} \dfrac{V_{12}}{xZ_L} + \dfrac{V_{34}}{yZ_L} = \dfrac{V - V_{12} - V_{34}}{(a - x + b + a - y)\,Z_L} \\[3mm] y = kx \end{cases} \Rightarrow$$

$$\begin{cases} x = \dfrac{(2a + b)\,(kV_{12} + V_{34})}{k^2 V_{12} + kV + V_{34}} \\[3mm] y = \dfrac{(2a + b)\,(k^2 V_{12} + kV_{34})}{k^2 V_{12} + kV + V_{34}} \end{cases} \tag{13}$$

For position (6), the equivalent mobile power supplies V_{12} and V_{23} are added between nodes 1, 2 and 2, 3. Then, the estimated position of V_{12} from node 1 is x, and the estimated position of V_{23} from node 2 is y. Assuming $y = kx$, the values of x and y are as follows:

$$\begin{cases} \dfrac{V_{12}}{xZ_L} + \dfrac{V_{23}}{yZ_L} = \dfrac{V - V_{12} - V_{23}}{(a - x + a + b - y)\,Z_L} \\[3mm] y = kx \end{cases} \Rightarrow$$

$$\begin{cases} x = \dfrac{(2a + b)\,(kV_{12} + V_{23})}{k^2 V_{12} + kV + V_{23}} \\[3mm] y = \dfrac{(2a + b)\,(k^2 V_{12} + kV_{23})}{k^2 V_{12} + kV + V_{23}} \end{cases} \tag{14}$$

For position (7), the equivalent mobile power supplies V_{12}, V_{23}, and V_{34} are added between nodes 1, 2, 2, 3 and 3, 4, then the estimated position of V_{12} from node 1 is x. The estimated position of V_{23} from node 2 is y, and the estimated position of V_{34} from node 3 is z. Assuming $y = k_1 x$, $z = k_2 x$, the values of x, y, and z are as follows:

$$\begin{cases} \dfrac{V_{12}}{xZ_L} + \dfrac{V_{23}}{yZ_L} + \dfrac{V_{34}}{zZ_L} = \dfrac{V - V_{12} - V_{23} - V_{34}}{(a - x + b - y + a - z)\,Z_L} \\[3mm] y = k_1 x \\[2mm] z = k_2 x \end{cases} \Rightarrow$$

$$\begin{cases} x = \dfrac{(2a + b)}{(k_1 + k_2 + 1)} \\[3mm] y = \dfrac{k_1\,(2a + b)}{(k_1 + k_2 + 1)} \\[3mm] z = \dfrac{k_2\,(2a + b)}{(k_1 + k_2 + 1)} \end{cases} \tag{15}$$

It can be seen that after adding the hypothesis conditions $y = k_1 x$ and $z = k_2 x$ in the above value analysis of different estimated positions, the estimated positions of other mobile power sources can be directly obtained by knowing the estimated positions of one equivalent mobile power source in the circuit. Therefore, the estimation relationship between the positions of multiple mobile power sources in the circuit can simplify the complex calculation process of real-time positioning and improve the accuracy and precision of location estimation.

However, the disadvantage of the above method is that when $x \approx 0$, the values of y and z are also 0, so the location estimation of mobile power supply is not applicable to this extreme case. As the complexity of circuit topology increases, the number of mobile power supplies and nodes increases; the frequency of power supply movement increases; the real-time location of power supplies under normal conditions needs to consider the multi-node analysis method based on the spatial electromagnetic field distribution.

3. THE METHOD OF SPACE ELECTROMAGNETIC FIELD ANALYSIS FOR VARIABLE SPEED NODES

Taking Fig. 3 as an example, a method of spatial electromagnetic field analysis of variable speed nodes is proposed by converting the assumed condition equivalent to the position change of variable speed nodes. The principle is shown in Fig. 4.

In Fig. 4, the variable speed nodes 1 and 2 move upward in the arrow direction with speed v_1, such that $y = v_1 t$ and $S_1 = av_1 t$. The variable speed nodes 2 and 3 move right in the arrow direction at the speed v_2, such that $z = v_2 t$, $S_2 = bv_2 t$.
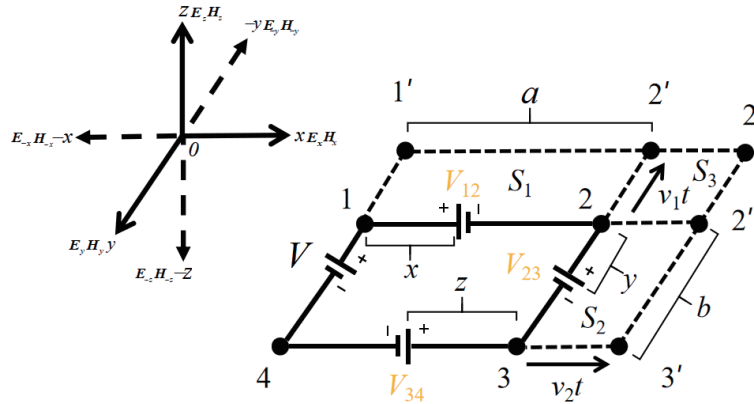
FIGURE 4. Schematic diagram of variable speed 4-node space electromagnetic field analysis method.

Variable speed nodes 1, 2, and 3 move up to the right in the arrow direction at speed v_1, such that $y = v_1t$, $z = v_2t$, $S_3 = v_1v_2t^2$. As the position of the variable speed node changes, the area of the space electromagnetic field passing through the closed circuit also changes accordingly, as shown in Equation (16).

$$\begin{cases} \dfrac{V_{12}}{xZ_L} + \dfrac{V_{23}}{yZ_L} + \dfrac{V_{34}}{zZ_L} = \dfrac{V - V_{12} - V_{23} - V_{34}}{(a - x + b - y + a - z)Z_L} \\[2mm] y = v_1t \\ z = v_2t \\ S_1 = av_1t \\ S_2 = bv_2t \\ S_3 = v_1v_2t^2 \end{cases} \quad (16)$$

As the speed and position of the variable node change dramatically, $y \gg x$, $z \gg x$. When $x \approx 0$, the values of y and z can be simplified to:

$$\begin{cases} y = 2a + b - z \\[2mm] z = \dfrac{(2a + b)}{2} \pm \dfrac{\sqrt{(2a + b)^2 - 4S_3}}{2} \end{cases} \quad (19)$$

It can be seen from Equation (19) that the variation trend of y and z is related to the sizes of S_3 and $2a + b$, as shown in Fig. 5.

As can be seen from the figure, y and z increase as the area of S_3 increases. In addition, the rate of change of y and z is also increasing. However, as $2a + b$ increases, the final values of y and z first become larger and then smaller, and the estimated position has a maximum value. This also means that the estimated position of the mobile power supply is gradually unaffected by

Let $V_{23} = dB * S_1/dt$, $V_{34} = dB * S_2/dt$, $y = v_1t$, $z = v_2t$ substitute into Equation (16) to get:

$$\frac{V_{12}}{xZ_L} + \frac{dB * a}{Z_L dt} + \frac{dB * b}{Z_L dt}$$

$$= \frac{V - V_{12} - \dfrac{dB * av_1t}{dt} - \dfrac{dB * bv_2t}{dt}}{(a - x + b - v_1t + a - v_2t)Z_L} \quad (17)$$

Discussed by case, when $dB/dt = k$ (constant), y and z can be solved by Equation (17) as follows:

$$\begin{cases} y = \dfrac{(2a+b)(V_{12}+kax+kbx)-(V+kax+kbx)x-(V_{12}+kax)z}{(V_{12}+kbx)} \\[3mm] z = \dfrac{(2a+b)(V_{12}+kax+kbx)-(V+kax+kbx)x \pm \sqrt{[(Vx+kax^2+kbx^2)-(2a+b)(V_{12}+kax+kbx)]^2-4S_3(V_{12}+kax)(V_{12}+kbx)}}{2(V_{12}+kax)} \end{cases} \quad (18)$$

the change in y and z values as $2a + b$ increases, depending only on the position of the variable speed node. Therefore, the variable speed node space electromagnetic field analysis method can realize the decoupling relationship between the estimated position of the mobile power supply and the y and z numerical calculation, and simplify the calculation method of the estimated position.

4. SIMULATION ANALYSIS

Figure 6 shows the comparison results of different $2a + b$ positions estimated by Equations (18) and (15) when S_3 changes continuously with k_1 and k_2. It can be seen that with the increase of $2a + b$, the error of the estimation results of the two methods decreases, and the final results gradually tend to be consistent. The arithmetic accuracy of position estimation using the variable speed node space electromagnetic field method is also illustrated.
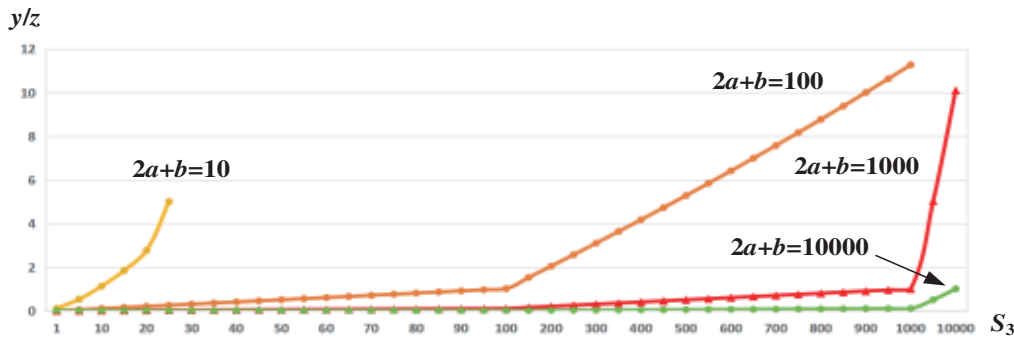
FIGURE 5. Relation curve between y and z position estimation of electromagnetic field in space of variable speed node and S_3.
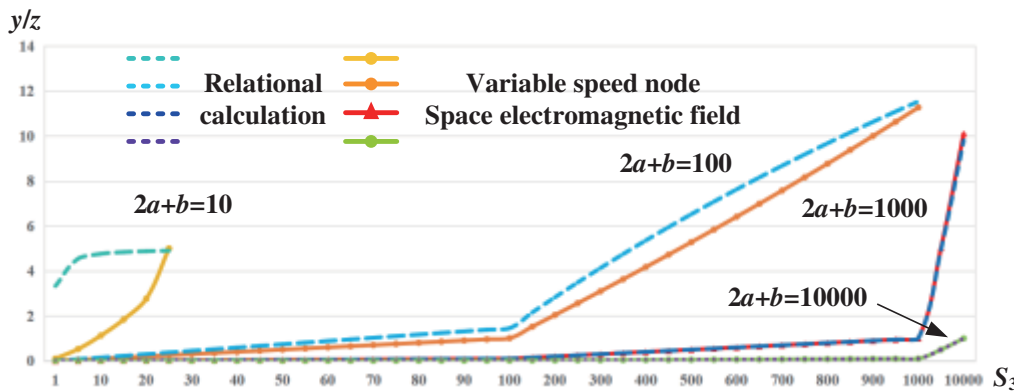
FIGURE 6. Comparison curves of position estimation results of different $2a + b$ under continuous changes of S_3, k_1 and k_2 under Equations (18) and (15).

Figure 7 shows the comparison results of position estimation of different S_3, k_1, and k_2 when $2a+b$ is continuously changed by Equations (18) and (15). Depending on S_3, the $2a + b$ range at which y and z reach their maximum is also different. The larger the area of S_3 is, the smaller the variation range of $2a+b$ is, and the greater the effect of S_3 is on the change of y and z. However, the difference of k_1 and k_2 has little effect on the change of y and z. This shows that the variable speed node space electromagnetic field method is more effective than the relational calculation method to obtain the estimated position.

When $2a+b$, S_3, k_1, and k_2 change continuously at the same time, the comparative results of position estimation of the two methods are shown in Figure 8. It can be clearly seen from the figure that with the increase of $2a + b$ value, y and z gradually reach the maximum value when $2a + b > 100$. The variable speed node space electromagnetic field method can obtain the ideal estimation position faster than the relational calculation method.

The current ratio is used to calculate the efficiency value by the voltage ratio. The circuit efficiency in the case of equal ratio is shown as follows. The circuit efficiencies of the two methods under Equation (8) are compared as shown in Figure 9.

As can be seen from the comparison of circuit efficiency in Figure 9, as the value of $2a + b$ increases, the circuit efficiency gradually becomes stable and reaches the maximum value. For optimal location estimation, $V_{23}/V = V_{34}/V = 0.1$, $V_{23}/V = V_{34}/V = 0.2$, $V_{23}/V = V_{34}/V = 0.3$, the variable speed node

space electromagnetic field method can obtain higher circuit efficiency than the relational calculation method from the aspect of circuit efficiency.

The above is a comparison of the position estimation of multiple mobile power sources discussed in the case of 4-node circuits. If the number of nodes is increased or decreased, assuming that the number of nodes is n, when $n = 5, 6, \ldots, m$, the comparison of location estimation of multiple mobile power sources in other cases is discussed.

When $n = 5, 6$, the principle diagram of the electromagnetic field analysis method of variable speed 5, 6 node space is shown in Figure 10.

In Figure 10, when the node is 5, the variable speed nodes 1 and 2 move upward in the arrow direction at the speed v_1, such that $y = v_1 t$, $S_1 = \frac{(a+f)\sqrt{v_1^2 t^2 - (a-f)^2}}{2}$; the variable speed node 3 moves to the right at the speed v_2 in the arrow direction such that $z = v_2 t$, $S_2 = \frac{v_2 t(b + v_1 t)}{2}$; variable speed node 4 moves right at speed v_3 in the arrow direction such that $e = v_3 t$, $S_3 = \frac{v_3 t \sqrt{(c + v_2 t)^2 - v_3^2 t^2}}{2}$. When the node is 6, the variable speed nodes 1 and 2 move upward in the arrow direction at the speed v_1, such that $y = v_1 t$, $S_1 = \frac{(a+f)\sqrt{v_1^2 t^2 - (a-f)^2}}{2}$; the variable speed node 3 moves up in the arrow direction with the speed v_2, such that $z = v_2 t$, $S_2 = \frac{v_2 t \sqrt{(b + v_1 t)^2 - v_2^2 t^2}}{2}$; variable

15
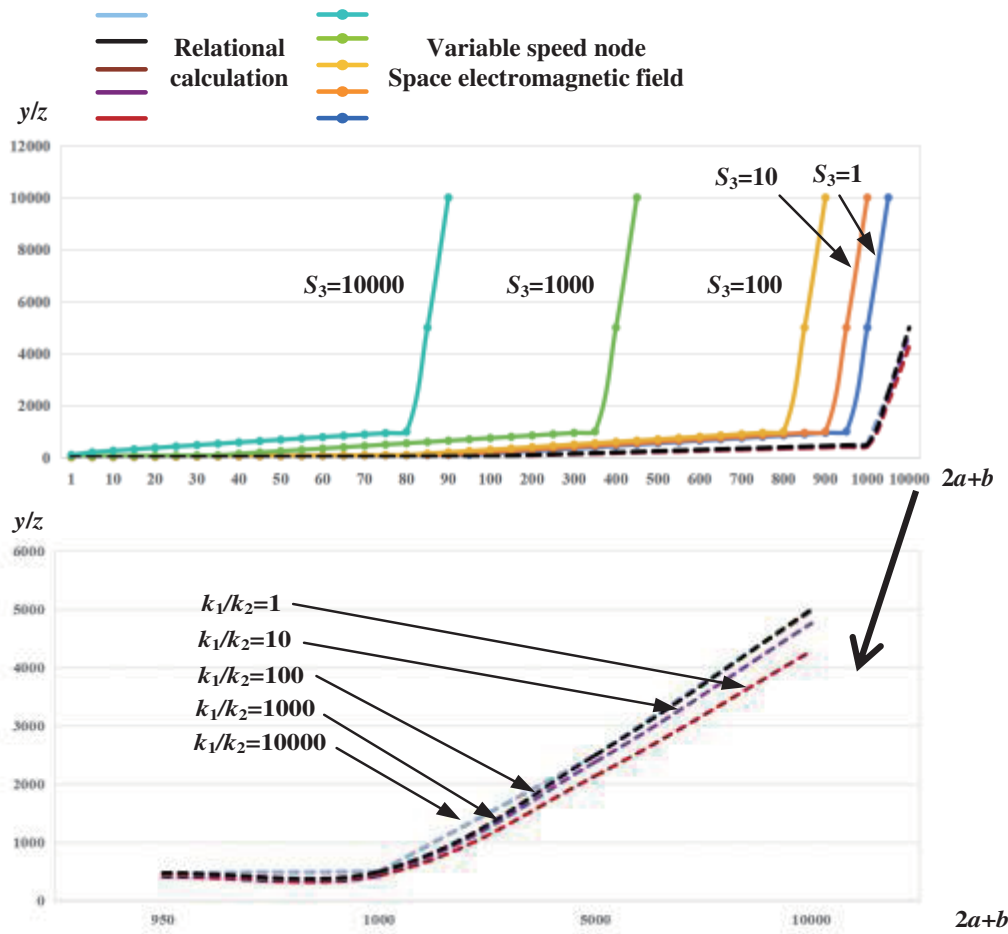
FIGURE 7. (18) and (15) Comparison curves of position estimation results of different S_3, k_1 and k_2 when $2a + b$ changes continuously.
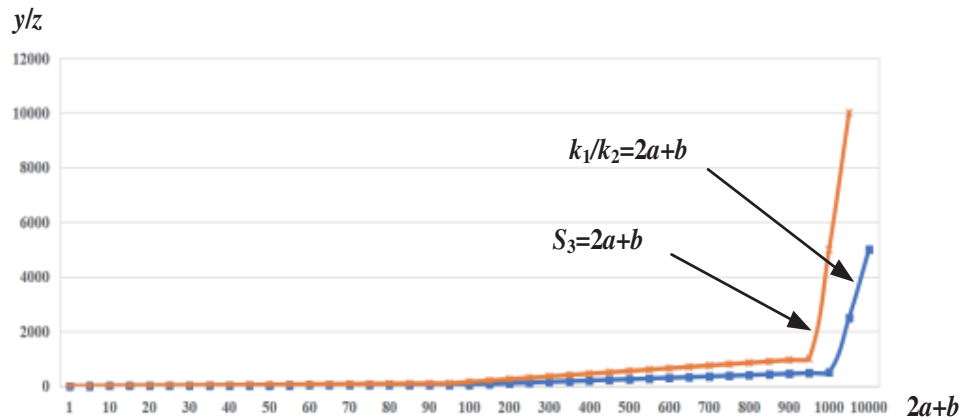
FIGURE 8. Comparison curves of position estimation results of Equations (18) and (15) under continuous changes of $2a + b$, S_3, k_1 and k_2.

speed node 4 moves to the right in the arrow direction at speed v_3, such that $e = v_3 t$, $S_3 = \frac{v_3 t \sqrt{(c+v_2 t)^2 - v_3^2 t^2}}{2}$; the variable speed node 5 moves right in the arrow direction with speed v_4, such that $h = v_4 t$, $S_4 = \frac{v_4 t \sqrt{(d+v_3 t)^2 - v_4^2 t^2}}{2}$. As the position of the variable speed node changes, the area of the space electro-magnetic field passing through the closed circuit also changes

accordingly. As shown in Equation (20) and Equation (21).

$$\begin{cases} \frac{V_{12}}{xZ_L} + \frac{V_{23}}{yZ_L} + \frac{V_{34}}{zZ_L} + \frac{V_{45}}{eZ_L} = \frac{V - V_{12} - V_{23} - V_{34} - V_{45}}{(a-x+b-v_1 t+c-v_2 t+d-v_3 t)Z_L} \\ y = v_1 t \\ z = v_2 t \\ e = v_3 t \\ S_1 = \frac{(a+f)\sqrt{v_1^2 t^2 - (a-f)^2}}{2} \\ S_2 = \frac{v_2 t(b+v_1 t)}{2} \\ S_3 = \frac{v_3 t\sqrt{(c+v_2 t)^2 - v_3^2 t^2}}{2} \end{cases}$$
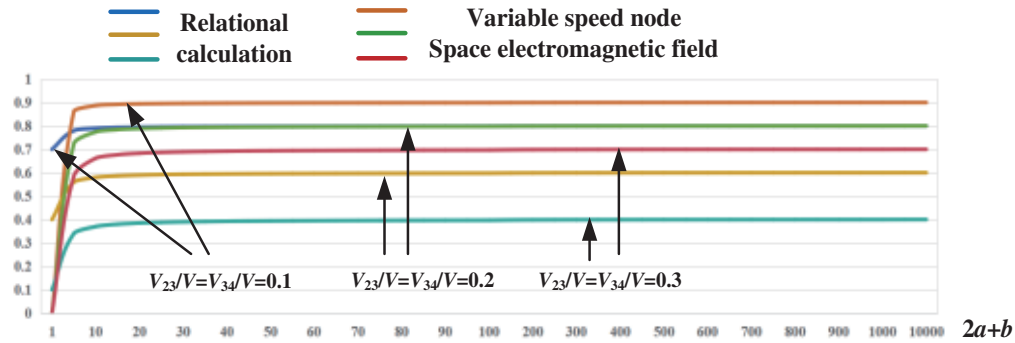
FIGURE 9. Circuit efficiency comparison results curve at $2a + b$, $V_{23}/V = V_{34}/V$ continuous changes.
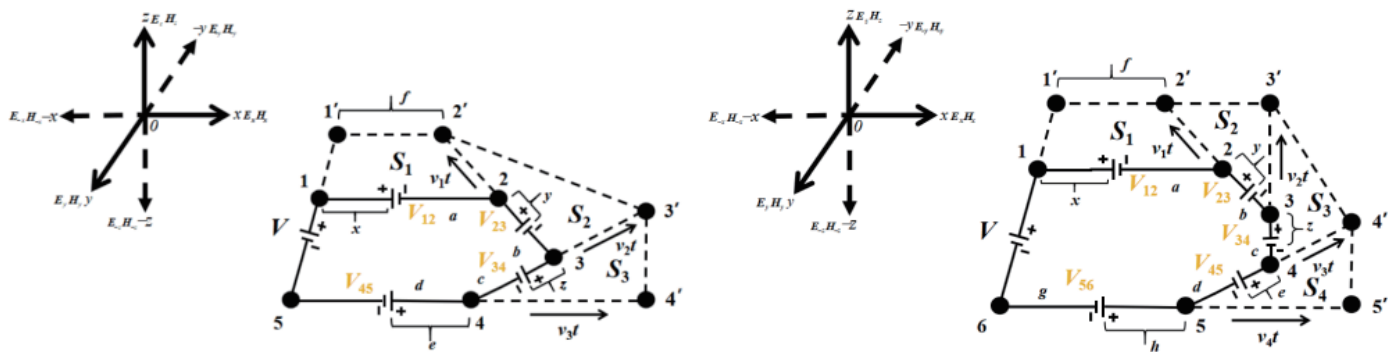
FIGURE 10. Schematic diagram of electromagnetic field analysis method for variable speed 5 and 6 nodes.
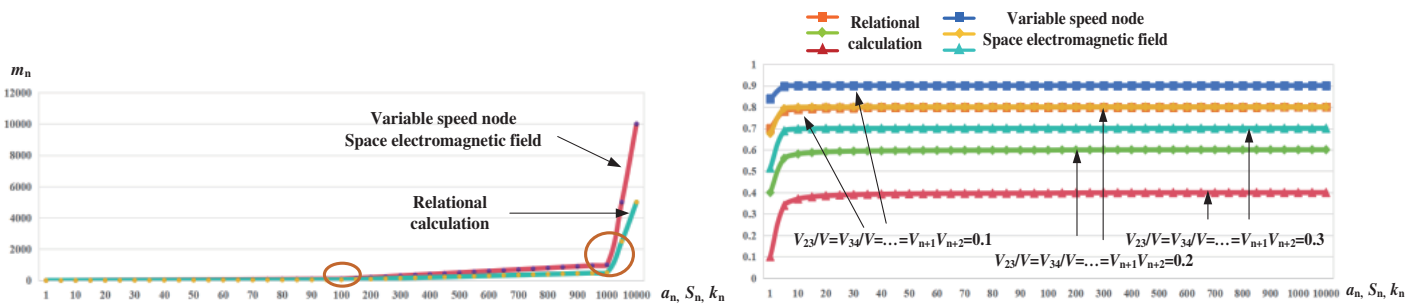
FIGURE 11. (23) Position estimation and circuit efficiency comparison results curve when a_n, S_n and k_n continuously change.

$$\Rightarrow \begin{cases} y+z+e=a+b+c+d \\ y=\sqrt{\dfrac{4S_1^2+(a-f)^4}{(a+f)^2}} \\ z=\dfrac{2S_2}{\sqrt{\dfrac{4S_1^2+(a-f)^4}{(a+f)^2}}+b} \\ e=a+b+c+d-y-z\approx\dfrac{2S_3}{c+\dfrac{2S_2}{\sqrt{\dfrac{4S_1^2+(a-f)^4}{(a+f)^2}}+b}} \end{cases} \quad (20)$$

$$\begin{cases} \dfrac{V_{12}}{xZ_L}+\dfrac{V_{23}}{yZ_L}+\dfrac{V_{34}}{zZ_L}+\dfrac{V_{45}}{eZ_L}+\dfrac{V_{56}}{hZ_L} \\ =\dfrac{V-V_{12}-V_{23}-V_{34}-V_{45}-V_{56}}{(a-x+b-v_1t+c-v_2t+d-v_3t+g-v_4t)\,Z_L} \\ y=v_1t \\ z=v_2t \\ e=v_3t \\ h=v_4t \\ S_1=\dfrac{(a+f)\sqrt{v_1^2t^2-(a-f)^2}}{2} \\ S_2=\dfrac{v_2t\sqrt{(b+v_1t)^2-v_2^2t^2}}{2} \\ S_3=\dfrac{v_3t\sqrt{(c+v_2t)^2-v_3^2t^2}}{2} \\ S_4=\dfrac{v_4t\sqrt{(d+v_3t)^2-v_4^2t^2}}{2} \end{cases}$$

17

$$\Rightarrow \begin{cases} y = \sqrt{\dfrac{4S_1^2 + (a-f)^4}{(a+f)^2}} \\[4mm] z \approx \dfrac{2S_2}{(b+y)} \approx \dfrac{2S_2}{b + \sqrt{\dfrac{4S_1^2+(a-f)^4}{(a+f)^2}}} \\[8mm] e \approx \dfrac{2S_3}{(c+z)} \approx \dfrac{2S_3}{c + \dfrac{2S_2}{b + \sqrt{\dfrac{4S_1^2+(a-f)^4}{(a+f)^2}}}} \\[10mm] h \approx \dfrac{2S_4}{(d+e)} \approx \dfrac{2S_4}{d + \dfrac{2S_3}{c + \dfrac{2S_2}{b + \sqrt{\dfrac{4S_1^2+(a-f)^4}{(a+f)^2}}}}} \end{cases} \quad (21)$$

In the above cases, the relational calculation method also has Equations (22) and (23).

$$\begin{cases} \dfrac{V_{12}}{xZ_L} + \dfrac{V_{23}}{yZ_L} + \dfrac{V_{34}}{zZ_L} + \dfrac{V_{45}}{eZ_L} = \dfrac{V-V_{12}-V_{23}-V_{34}-V_{45}}{(a-x+b-y+c-z+d-e)Z_L} \\ y = k_1 x \\ z = k_2 x \\ e = k_3 x \end{cases}$$

$$\Rightarrow \begin{cases} x = \dfrac{(a+b+c+d)}{\dfrac{(V-V_{12}-V_{23}-V_{34}-V_{45})}{\left(V_{12}+\frac{V_{23}}{k_1}+\frac{V_{34}}{k_2}+\frac{V_{45}}{k_3}\right)}+(1+k_1+k_2+k_3)} \\[8mm] y = \dfrac{k_1(a+b+c+d)}{\dfrac{(V-V_{12}-V_{23}-V_{34}-V_{45})}{\left(V_{12}+\frac{V_{23}}{k_1}+\frac{V_{34}}{k_2}+\frac{V_{45}}{k_3}\right)}+(1+k_1+k_2+k_3)} \\[8mm] z = \dfrac{k_2(a+b+c+d)}{\dfrac{(V-V_{12}-V_{23}-V_{34}-V_{45})}{\left(V_{12}+\frac{V_{23}}{k_1}+\frac{V_{34}}{k_2}+\frac{V_{45}}{k_3}\right)}+(1+k_1+k_2+k_3)} \\[8mm] e = \dfrac{k_3(a+b+c+d)}{\dfrac{(V-V_{12}-V_{23}-V_{34}-V_{45})}{\left(V_{12}+\frac{V_{23}}{k_1}+\frac{V_{34}}{k_2}+\frac{V_{45}}{k_3}\right)}+(1+k_1+k_2+k_3)} \end{cases}$$

$$(22)$$

$$\begin{cases} \dfrac{V_{12}}{xZ_L} + \dfrac{V_{23}}{yZ_L} + \dfrac{V_{34}}{zZ_L} + \dfrac{V_{45}}{eZ_L} + \dfrac{V_{56}}{hZ_L} = \dfrac{V-V_{12}-V_{23}-V_{34}-V_{45}-V_{56}}{(a-x+b-y+c-z+d-e+g-h)Z_L} \\ y = k_1 x \\ z = k_2 x \\ e = k_3 x \\ h = k_4 x \end{cases}$$

$$\Rightarrow \begin{cases} x = \dfrac{(a+b+c+d+g)}{\frac{(V-V_{12}-V_{23}-V_{34}-V_{45}-V_{56})}{\left(V_{12}+\frac{V_{23}}{k_1}+\frac{V_{34}}{k_2}+\frac{V_{45}}{k_3}+\frac{V_{56}}{k_4}\right)}+(1+k_1+k_2+k_3+k_4)} \\[6mm] y = \dfrac{k_1(a+b+c+d+g)}{\frac{(V-V_{12}-V_{23}-V_{34}-V_{45}-V_{56})}{\left(V_{12}+\frac{V_{23}}{k_1}+\frac{V_{34}}{k_2}+\frac{V_{45}}{k_3}+\frac{V_{56}}{k_4}\right)}+(1+k_1+k_2+k_3+k_4)} \\[6mm] z = \dfrac{k_2(a+b+c+d+g)}{\frac{(V-V_{12}-V_{23}-V_{34}-V_{45}-V_{56})}{\left(V_{12}+\frac{V_{23}}{k_1}+\frac{V_{34}}{k_2}+\frac{V_{45}}{k_3}+\frac{V_{56}}{k_4}\right)}+(1+k_1+k_2+k_3+k_4)} \\[6mm] e = \dfrac{k_3(a+b+c+d+g)}{\frac{(V-V_{12}-V_{23}-V_{34}-V_{45}-V_{56})}{\left(V_{12}+\frac{V_{23}}{k_1}+\frac{V_{34}}{k_2}+\frac{V_{45}}{k_3}+\frac{V_{56}}{k_4}\right)}+(1+k_1+k_2+k_3+k_4)} \\[6mm] h = \dfrac{k_4(a+b+c+d+g)}{\frac{(V-V_{12}-V_{23}-V_{34}-V_{45}-V_{56})}{\left(V_{12}+\frac{V_{23}}{k_1}+\frac{V_{34}}{k_2}+\frac{V_{45}}{k_3}+\frac{V_{56}}{k_4}\right)}+(1+k_1+k_2+k_3+k_4)} \end{cases} \quad (23)$$

As the number of nodes increases to m, the general formula for estimating the position of multiple mobile power sources using two methods can be directly expressed as follows:

$$\begin{cases} m_1 = \sqrt{\dfrac{4S_1^2 + (a_1-f)^4}{(a_1+f)^2}} \\[4mm] m_2 \approx \dfrac{2S_2}{(a_2+m_1)} \approx \dfrac{2S_2}{a_2 + \sqrt{\dfrac{4S_1^2+(a_1-f)^4}{(a_1+f)^2}}} \\[8mm] m_3 \approx \dfrac{2S_3}{(a_3+m_2)} \approx \dfrac{2S_3}{a_3 + \dfrac{2S_2}{a_2 + \sqrt{\dfrac{4S_1^2+(a_1-f)^4}{(a_1+f)^2}}}} \\[10mm] m_4 \approx \dfrac{2S_4}{(a_4+m_3)} \approx \dfrac{2S_4}{a_4 + \dfrac{2S_3}{a_3 + \dfrac{2S_2}{a_2 + \sqrt{\dfrac{4S_1^2+(a_1-f)^4}{(a_1+f)^2}}}}} \\[4mm] \vdots \\ m_n \approx \dfrac{2S_n}{(a_n+m_{n-1})} \\[4mm] \approx \dfrac{2S_n}{a_n + \dfrac{2S_{n-1}}{a_{n-1}+\cdots+\dfrac{2S_4}{a_4+\dfrac{2S_3}{a_3+\dfrac{2S_2}{a_2+\sqrt{\frac{4S_1^2+(a_1-f)^4}{(a_1+f)^2}}}}}}} \end{cases} \quad (24)$$

$$\begin{cases} m_1 = \dfrac{k_1(a_1+a_2+a_3+a_4+a_5)}{\frac{(V-V_{12}-V_{23}-V_{34}-V_{45}-V_{56})}{\left(V_{12}+\frac{V_{23}}{k_1}+\frac{V_{34}}{k_2}+\frac{V_{45}}{k_3}+\frac{V_{56}}{k_4}\right)}+(1+k_1+k_2+k_3+k_4)} \\[6mm] m_2 = \dfrac{k_2(a_1+a_2+a_3+a_4+a_5)}{\frac{(V-V_{12}-V_{23}-V_{34}-V_{45}-V_{56})}{\left(V_{12}+\frac{V_{23}}{k_1}+\frac{V_{34}}{k_2}+\frac{V_{45}}{k_3}+\frac{V_{56}}{k_4}\right)}+(1+k_1+k_2+k_3+k_4)} \\[6mm] m_3 = \dfrac{k_3(a_1+a_2+a_3+a_4+a_5)}{\frac{(V-V_{12}-V_{23}-V_{34}-V_{45}-V_{56})}{\left(V_{12}+\frac{V_{23}}{k_1}+\frac{V_{34}}{k_2}+\frac{V_{45}}{k_3}+\frac{V_{56}}{k_4}\right)}+(1+k_1+k_2+k_3+k_4)} \\[6mm] m_4 = \dfrac{k_4(a_1+a_2+a_3+a_4+a_5)}{\frac{(V-V_{12}-V_{23}-V_{34}-V_{45}-V_{56})}{\left(V_{12}+\frac{V_{23}}{k_1}+\frac{V_{34}}{k_2}+\frac{V_{45}}{k_3}+\frac{V_{56}}{k_4}\right)}+(1+k_1+k_2+k_3+k_4)} \\[4mm] \vdots \\ m_n = \dfrac{k_n(a_1+a_2+a_3+a_4+a_5+\cdots+a_{n+1})}{\frac{(V-V_{12}-V_{23}-V_{34}-V_{45}-V_{56}-\cdots-V_{n+1\,n+2})}{\left(V_{12}+\frac{V_{23}}{k_1}+\frac{V_{34}}{k_2}+\frac{V_{45}}{k_3}+\frac{V_{56}}{k_4}+\cdots+\frac{V_{n+1\,n+2}}{k_n}\right)}+(1+k_1+k_2+k_3+k_4+\cdots+k_n)} \end{cases}$$

$$(25)$$

When the number of circuit nodes increases to m, the comparison between the two methods for the estimated positions of multiple mobile power sources is shown in Figure 11.

As can be seen from Figure 11, with the continuous increase of a_n, S_n, and k_n, the number of nodes increases to m, and the influence of the estimated position of multiple mobile power supplies on circuit efficiency obtained by using the spatial electromagnetic field analysis method of variable speed nodes still conforms to the previous analysis results. It can also be seen from the change trend curve of m_n in position estimation that

when a_n, S_n, and k_n increase to the two key turning points of 100 and 1000, the spatial electromagnetic field analysis method of variable speed node can predict the moving position of multiple mobile power sources faster and more accurately than the relational calculation method.

5. CONCLUSION

In order to analyze the influence of position transformation and displacement rate of multiple mobile high frequency power supplies on the output power and efficiency of each node in the system, the spatial electromagnetic field analysis method of variable speed node can realize the decoupling relationship between the estimated position of the mobile power supply and the numerical calculation of the relationship, and simplify the calculation method of the estimated position. In terms of circuit efficiency, the variable speed node space electromagnetic field method can obtain higher circuit efficiency than the relational calculation method. This method is conducive to the future study of dynamic spatial electromagnetic characteristics of multi-node and multi-mobile high-frequency power supply systems under variable speed physical field coupling, and the dynamic parameters of circuit topology and node output power characteristics are combined as the research content.

REFERENCES

[1] Ye, Z., C. Chen, B. Chen, and K. Wu, "Resilient service restoration for unbalanced distribution systems with distributed energy resources by leveraging mobile generators," *IEEE Transactions on Industrial Informatics*, Vol. 17, No. 2, 1386–1396, 2021.

[2] Yan, M., M. Shahidehpour, A. Paaso, L. Zhang, A. Alabdulwahab, and A. Abusorrah, "Distribution system resilience in ice storms by optimal routing of mobile devices on congested roads," *IEEE Transactions on Smart Grid*, Vol. 12, No. 2, 1314–1328, 2021.

[3] Taheri, B., A. Safdarian, M. Moeini-Aghtaie, and M. Lehtonen, "Distribution system resilience enhancement via mobile emergency generators," *IEEE Transactions on Power Delivery*, Vol. 36, No. 4, 2308–2319, 2021.

[4] Liu, C. H., Z. Dai, Y. Zhao, J. Crowcroft, D. Wu, and K. K. Leung, "Distributed and energy-efficient mobile crowdsensing with charging stations by deep reinforcement learning," *IEEE Transactions on Mobile Computing*, Vol. 20, No. 1, 130–146, 2021.

[5] Rodrigues, F. M., L. R. Araujo, and D. R. R. Penido, "A method to improve distribution system reliability using available mobile generators," *IEEE Systems Journal*, Vol. 15, No. 3, 4635–4643, 2021.

[6] Huang, D., B. Chen, T. Huang, X. Fang, H. Zhang, and J. Cao, "Open capacity enhancement model of medium voltage distribution network with mobile energy storage system," *IEEE Access*, Vol. 8, 205 061–205 070, 2020.

[7] Erenoğlu, A. K. and O. Erdinç, "Real-time allocation of multi-mobile resources in integrated distribution and transportation systems for resilient electrical grid," *IEEE Transactions on Power Delivery*, Vol. 38, No. 2, 1108–1119, 2023.

[8] Han, D., B. Zheng, Z. Chen, and S. Li, "Cost efficiency in coordinated multiple-point system based on multi-source power supply," *IEEE Access*, Vol. 6, 71 994–72 001, 2018.

[9] Saito, H., "Theoretical analysis of nonlinear energy harvesting from wireless mobile nodes," *IEEE Wireless Communications Letters*, Vol. 10, No. 9, 1914–1918, 2021.

[10] Liu, J., K. Xiong, P. Fan, and Z. Zhong, "Resource allocation in wireless powered sensor networks with circuit energy consumption constraints," *IEEE Access*, Vol. 5, 22 775–22 782, 2017.

[11] Tong, L., S. Zhao, H. Jiang, J. Zhou, and B. Xu, "Multi-scenario and multi-objective collaborative optimization of distribution network considering electric vehicles and mobile energy storage systems," *IEEE Access*, Vol. 9, 55 690–55 697, 2021.

[12] Samara, S., M. F. Shaaban, and A. H. Osman, "Optimal management of mobile energy generation and storage systems," *IEEE Access*, Vol. 8, 203 890–203 900, 2020.

[13] Jagadeesh, G. R. and T. Srikanthan, "Online map-matching of noisy and sparse location data with hidden markov and route choice models," *IEEE Transactions on Intelligent Transportation Systems*, Vol. 18, No. 9, 2423–2434, 2017.

[14] Zhou, S., Y. Qiu, F. Zou, D. He, P. Yu, J. Du, X. Luo, C. Wang, Z. Wu, and W. Gu, "Dynamic EV charging pricing methodology for facilitating renewable energy with consideration of highway traffic flow," *IEEE Access*, Vol. 8, 13 161–13 178, 2019.

[15] Liu, F., H. Lu, T. Wang, and Y. Liu, "An energy-balanced joint routing and charging framework in wireless rechargeable sensor networks for mobile multimedia," *IEEE Access*, Vol. 7, 177 637–177 650, 2019.

[16] Chen, H., Z. Su, Y. Hui, and H. Hui, "Dynamic charging optimization for mobile charging stations in internet of things," *IEEE Access*, Vol. 6, 53 509–53 520, 2018.

[17] Kokubo, T., S. Yamasaki, and M. Nakagawa, "Transmission delay control for single frequency OFDM multi-base-station in a cell using position information," in *Vehicular Technology Conference Fall 2000. IEEE VTS Fall VTC2000. 52nd Vehicular Technology Conference (Cat. No.00CH37152)*, Vol. 2, 524–529, Boston, MA, USA, 2000.

[18] Kotikot, S. M., B. Kar, and O. A. Omitaomu, "A geospatial framework using multicriteria decision analysis for strategic placement of reserve generators in Puerto Rico," *IEEE Transactions on Engineering Management*, Vol. 67, No. 3, 659–669, 2020.

[19] Cheng, Z.-H., T. Li, L. Hu, X. Ma, F. Liang, D. Zhao, and B.-Z. Wang, "Selectively powering multiple small-size devices spaced at diffraction limited distance with point-focused electromagnetic waves," *IEEE Transactions on Industrial Electronics*, Vol. 69, No. 12, 13 696–13 705, 2021.

[20] Slone, R. D., J.-F. Lee, and R. Lee, "Multipoint Galerkin asymptotic waveform evaluation," in *IEEE Antennas and Propagation Society International Symposium. Transmitting Waves of Progress to the Next Millennium. 2000 Digest. Held in Conjunction with: USNC/URSI National Radio Science Meeting (C*, Vol. 4, 2356–2359, Salt Lake City, UT, USA, 2000.

[21] Watanabe, K., M. Komatsu, M. Aoi, R. Sakai, S. Tanaka, and M. Nagata, "Analysis of electromagnetic noise from switching power modules using wide band gap semiconductors," *IEEE Letters on Electromagnetic Compatibility Practice and Applications*, Vol. 4, No. 4, 92–96, 2022.

[22] Li, Q., Y.-Z. Xie, K.-J. Li, and X. Kong, "A portable electric field detector with precise time base for transient electromagnetic radiation source location," *IEEE Transactions on Instrumentation and Measurement*, Vol. 69, No. 4, 1408–1415, 2020.

[23] Wang, T., M. Gao, J. Huang, Y. Zhu, F. Wang, and M. Zhang, "Finite element analysis of electromagnetic vibration in large capacity on-board transformer," in *2022 Power System and Green Energy Conference (PSGEC)*, 1111–1117, Shanghai, China, 2022.

[24] Yi, J., P. Yang, Z. Li, P. Kong, and J. Li, "Mutual inductance calculation of circular coils for an arbitrary position with a finite magnetic core in wireless power transfer systems," *IEEE Transactions on Transportation Electrification*, Vol. 9, No. 1, 1950–1959, 2023.

[25] Zhang, R., Y. Wang, and H. Xu, "A novel analytical method suitable for coupled electromagnetic field of circuit," *Progress In Electromagnetics Research M*, Vol. 100, 35–50, 2021.